Journal of Dental Research
2026, Vol. 105(3) 385–395


Article reuse guidelines:
sagepub.com/journals-permissions
DOI: 10.1177/00220345251349109
journals.sagepub.com/home/jdr

The Absence of Claudin-10 in the Enamel Organ Alters Its Integrity

T.N. Nguyen[1*], S. Ribes[1*], C. Andrique[1], M. Requin[2], J. Bouchet[1], N. Obtel[1,3], L. Slimani[1], N. Brouilly[2], C. Torrens[1], A. Schmitt[4], T. Guilbert[4], M. Morawietz[5], A. Kiesow[5], A. Brunelle[6], A. Percot[7], S. Hadj-Rabia[8], C. Gaucher[1,3], A. Le Bivic[2], P. Houillier[9,10], C. Bardet[1], D. Muller[11], F. Ramirez Rozzi[1,12], T. Coradin[13], T. Breiderhoff[11,14], and C. Chaussain[1,3]

Abstract

Rare disorders related to tight junction (TJ) proteins have been associated with amelogenesis imperfecta. Pathogenic variants of *CLDN10*, encoding claudin-10b, a cation transport pore, cause the autosomal recessive HELIX syndrome (Hypohidrosis, Electrolyte imbalance, hypoLacrymia, Ichthyosis, Xerostomia). Patients exhibit salivary dysfunction and rapid enamel wear after tooth eruption. Since *Cldn10* is expressed in the dental epithelium, this study explores the role of claudin-10b in amelogenesis. We analyzed amelogenesis in constitutive and conditional *Cldn10* knockout (KO) murine models, comparing the findings to human HELIX enamel. First, analysis of constitutive *Cldn10* knockout (KO) mice, which die within a few hours after birth, showed that claudin-10 is present at the plasma membrane of the stratum intermedium but not at the TJs during the secretory stage. Its absence altered gene expression related to ion transport and pH control, although without major disturbance in cell polarization or enamel matrix synthesis. Examination of later stages of amelogenesis in epithelium-targeted conditional *Cldn10* KO mice showed that claudin-10 is present in the papillary layer at the maturation stage. In its absence, the pH of the enamel matrix was more basic during early maturation, suggesting that claudin-10 determines enamel matrix pH. However, at later stage of the maturation process, the pH was corrected and the resulting enamel did not show major structural or elemental alterations. These later findings were confirmed by exploring the enamel of *Cldn10* KO transplanted tooth germs, which have developed in a controlled mineral environment. Nevertheless, higher contents of aluminum were detected in the enamel of transplanted germs and in human HELIX enamel, suggesting that claudin-10 deficiency may lead to a loss of enamel organ integrity. These data suggest that while salivary dysfunction is the main cause of enamel wear in HELIX, claudin-10 plays a direct role in amelogenesis by determining pH and enamel organ integrity.

Keywords: Amelogenesis, Ameloblasts, Tight junctions, Ion transport, Aluminum, Genetic disorders

Introduction

Tight junctions (TJs) form the backbone of the paracellular pathway for epithelial ion transport. Recently, the paracellular pathway has been shown to be highly ion specific, tightly regulated, and causally involved in human diseases (Meoli and Gunzel 2023). The specific set of claudins expressed at each TJ is uniquely tailored to the tissue and is responsible for the permeability and selectivity properties of the TJ. Several rare disorders resulting from pathogenic variants in a gene encoding a claudin (*CLDN*) have been reported, most of which result in disturbances of the ion homeostasis in the kidney (Meoli and Gunzel 2023). We have previously reported that patients with familial hypomagnesemia with hypercalciuria and nephrocalcinosis due to mutations in *CLDN16* or *CLDN19* displayed amelogenesis imperfecta (AI) (Bardet et al. 2016; Yamaguti et al. 2017). Recently, a novel claudinopathy caused by pathogenic variants in *CLDN10* has been reported, resulting in the HELIX syndrome (Hypohidrosis, Electrolyte imbalance-renal loss of NaCl with secondary hyperaldosteronism and hypokalemia- hypoLacrymia, Ichthyosis, and Xerostomia) (Klar et al. 2017; Hadj-Rabia et al. 2018). HELIX patients complained of xerostomia (dry mouth) due to a 98% reduction in salivary flow rate compared with controls (Hadj-Rabia et al. 2018). Claudin-10 exists in 2 isoforms, resulting from 2 alternative exons, 1a and 1b (*CLDN10A*, *CLDN10B*) (Gunzel et al. 2009). *CLDN10B* encodes claudin-10b, an integral membrane-spanning protein of TJs expressed in the kidney thick ascending limb of Henle's loop (TAL), skin, and salivary glands (Breiderhoff et al. 2012; Milatz 2019; He et al. 2024) and also in the tooth germ (Ohazama and Sharpe 2007; Chiba et al. 2020; Wang et al. 2020). We diagnosed early tooth wear in the

6 HELIX patients reported in Hadj-Rabia et al. (2018). The teeth formed normally, but the enamel eroded rapidly after tooth eruption, suggesting that the enamel wear was mainly due to salivary dysfunction (Obtel et al. 2022). Since claudin-10b has been shown to be expressed in the mouse enamel organ (Chiba et al. 2020), a direct effect of its impairment on amelogenesis cannot be excluded. Therefore, this study aims to investigate the role of claudin-10b in amelogenesis. To this purpose, we studied constitutive and conditional *Cldn10* knockout (KO) mouse models, a kidney capsule tooth germ transplantation model (Jimenez-Rojo and Mitsiadis 2023), and human teeth (Obtel et al. 2022).

Materials and Methods

The detailed methodology is described in the Appendix Materials and Methods.

Results

Claudin-10 Is Expressed in the Stratum Intermedium at All Stages of Amelogenesis

Converging data have indicated that *Cldn10*/claudin-10 is expressed in the enamel organ at different locations and stages (Ohazama and Sharpe 2007; Chiba et al. 2020; Wang et al. 2020). In wild-type (WT) mice, both frontal and sagittal sections of the continuously growing incisor revealed claudin-10 labeling in the stratum intermedium (SI), throughout all stages of amelogenesis, from the cervical loop to the tip of the incisor at day 1 (P1) after birth (Fig. 1A, Appendix Fig. 1–2A). Similar labeling was observed in the secretory ameloblasts of the first molar germ (Appendix Fig. 2B). The specificity of claudin-10 immunostaining was validated using constitutive *Cldn10* KO mice (Appendix Fig. 3A). Co-labeling with the TJ protein ZO-1 showed the expression of claudin-10 in the SI but not at the TJs (Fig. 1A, Appendix Fig. 1). To clarify this later point, we performed stimulated emission depletion microscopy and confirmed that the expression of claudin-10 was restricted to the SI without co-labeling with ZO-1 (Fig. 1B and Appendix Fig. 3). Co-labeling with connexin-43, a marker for gap junctions that are abundant in the SI (Liu et al. 2016), also revealed no co-labeling with claudin-10 (Appendix Fig. 4). Next, we performed claudin-10 immunogold labeling and observed a positive signal in the plasma membranes of the SI but not associated with TJs (Fig. 1C; Appendix Fig. 5). Next, we assessed claudin-10 expression in the dental epithelium at the maturation stage in adult mice and observed positive labeling of the papillary layer (Fig. 1D).

The Ameloblast Layer Is Disturbed in Constitutive Cldn10 KO Pups

We next investigated constitutive *Cldn10* KO mice to study the impact of claudin-10 deficiency on the early stages of amelogenesis, considering that pups die a few hours after birth (Breiderhoff et al. 2012) (Fig. 2). Staining of sagittal sections from the continuously growing incisor revealed disorganization in both the secretory ameloblast layer and the SI in constitutive *Cldn10* KO mice (Fig. 2A, right panels). In contrast,

[1]Université Paris Cité, INSERM U1333 Santé Orale, et Plateforme Imagerie du Vivant (PIV), FHU-DDS-net, IHMOA, Dental School, Montrouge, France
[2]Aix Marseille Université, CNRS, IBDM-UMR7288, Marseille, France
[3]AP-HP Services de médecine bucco-dentaire, Hôpitaux Universitaires Bretonneau (CRMR phosphore et calcium, filière OSCAR et ERN BOND), and Henri Mondor and Charles Foix (filière TETECOU et ERN CRANIO), FHU DDS-net, Ile de France, France
[4]Université Paris Cité, Institut Cochin, INSERM U1016, CNRS UMR8104, Paris, France
[5]Fraunhofer Institute for Microstructure of Materials and Systems IMWS, Walter-Huelse-Straße 1, 06120 Halle, Germany
[6]Sorbonne Université, CNRS, Laboratoire d'Archéologie Moléculaire et Structurale, Paris, France
[7]Sorbonne Université, CNRS MONARIS UMR8233, 4 Place Jussieu, Paris, France
[8]Université Paris Cité, INSERM1163 Institut Imagine; APHP5, Hôpital Necker-Enfants Malades Dpt of Dermatology, Reference Center for rare skin diseases, Paris, France
[9]Université Paris Cité, Sorbonne Université, Centre de Recherche des Cordeliers, INSERM, CNRS-ERL8228, F-75006 Paris, France
[10]APHP, Service de Physiologie, Centre de Référence des Maladies Rénales Héréditaires de l'Enfant et de l'Adulte (MARHEA), Hôpital Européen Georges Pompidou, F-75015 Paris, France
[11]Charité Universitaets medizin Berlin, Department of Pediatrics, Division of Gastroenterology, Nephrology and Metabolic Diseases, Augustenburger Platz 1, Berlin, Germany
[12]Eco-anthropologie (EA), Muséum national d'Histoire naturelle, CNRS, Université de Paris, Musée de l'Homme 17 place du Trocadéro Paris, France
[13]Sorbonne Université, CNRS, Laboratoire de Chimie de la Matière Condensée de Paris, Paris, France
[14]German Center for Neurodegenerative Diseases (DZNE), Munich, Germany

*Authors contributing equally to this article.

A supplemental appendix to this article is available online.

Corresponding Authors:
Catherine Chaussain, INSERM, Université Paris Cité, 1 rue Maurice Arnoux, Montrouge, 92120, France.
Email: catherine.chaussain@u-paris.fr
Tilman Breiderhoff, Department of Pediatrics, Division of Gastroenterology, Nephrology and Metabolic Diseases, Charité Universitaets medizin Berlin, Campus Virchow-Klinikum | Augustenburger Platz 1, Berlin, 13353, Germany.
Email: tilman.breiderhoff@dzne.de

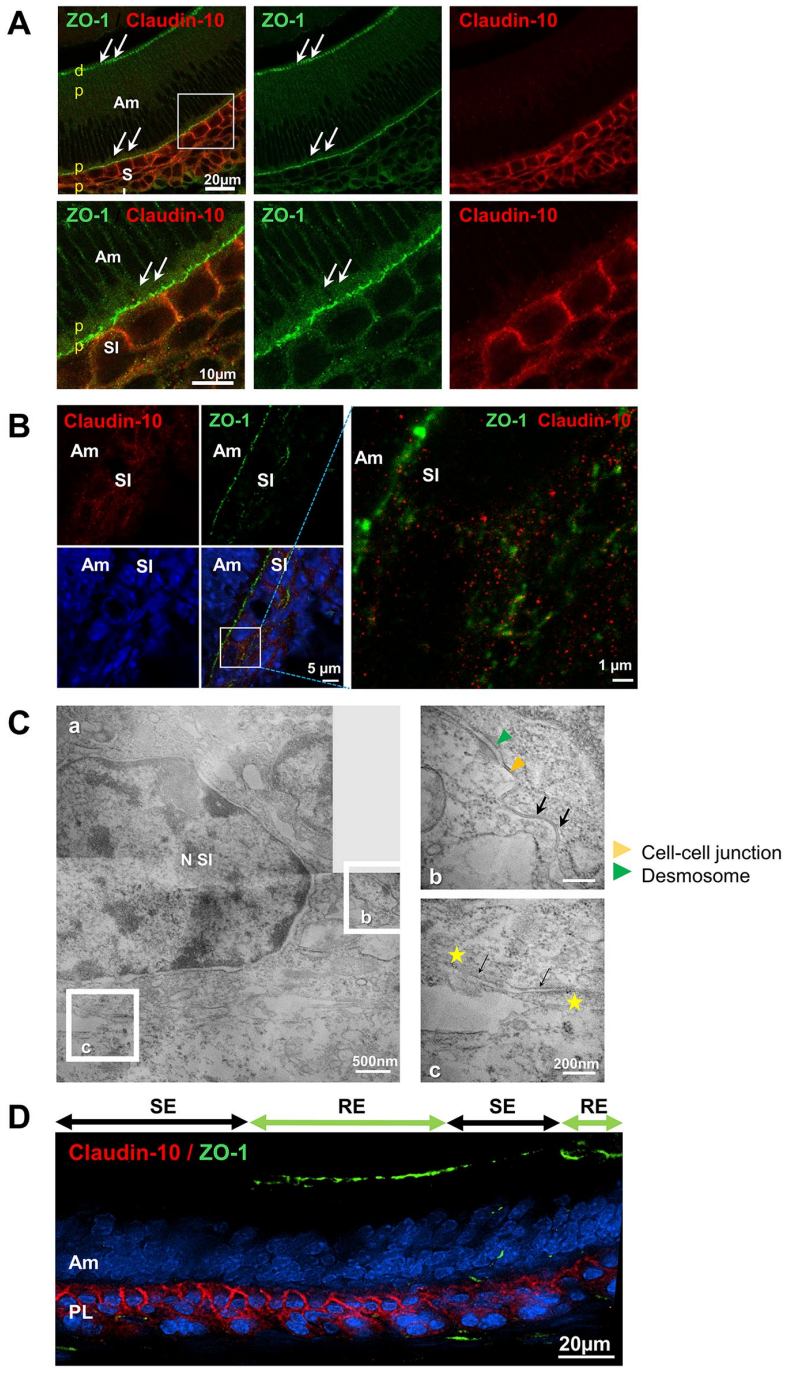

Figure 1. Claudin-10 expression profiling and protein identification in the wild-type (WT) murine incisor germ. (**A**) Localization of claudin-10 in the stratum intermedium. Top line: fluorescence microscopy shows the secretory ameloblasts (Am) alignment and, below, stratum intermedium (SI) lines. The tight junction (TJ)–associated protein zonula occludens-1 (ZO-1) in green was localized both at the distal and proximal end of ameloblasts (arrows). Arrows indicate TJs. Claudin-10 labeling (in red) is present only on the SI cell membrane. Bottom line: Inset of top line = proximal end of ameloblasts. Data show that there is no colocalization of claudin-10 and ZO-1 at the proximal TJ at this stage of postnatal day 1 (P1) WT murine germ. Am, ameloblasts; SI, stratum intermedium; dp, distal pole of ameloblast; pp, proximal pole of ameloblast. (**B**) Immunofluorescence analysis by stimulated emission depletion microscopy at postnatal day 1 showing no co-labeling between claudin-10 and ZO-1 and reveals that claudin-10 labeling is restricted to the SI. (**C**) Immunolocalization of claudin-10 in the stratum intermedium at postnatal day 1. Immunogold staining using anti–claudin-10 antibodies and 6-nm gold beads conjugated secondary antibodies on ultrathin sections (see the "Materials and Methods" section) of P1 WT mouse tooth. Beads (yellow stars) are detected only along the membranes of cells from the SI. Desmosomes and cell–cell junctions are indicated by green and orange arrowheads, respectively. Black arrows indicate membranes. (b) and (c) are enlarged views of (a). Scale bars are indicated. (**D**) At the maturation stage, ZO-1 immunolabeling (in green) is observed in the TJs located at the apical end of ruffle-ended ameloblasts (RA) and is absent in smooth-ended ameloblasts (SA) as SA remove their apical TJs (Lacruz et al., 2017). Claudin-10 labeling (in red) is present in both cases in in the papillary layer (3-mo-old adult mice). Am, ameloblasts; PL, papillary layer; SI, stratum intermedium; SI N, stratum intermedium nucleus.

littermate WT pups showed well-aligned ameloblasts (Fig. 2A, left panels). Amelogenin–positive forming enamel matrix was observed in both genotypes (Fig. 2A insets; Fig. 2B). Fluorescent labeling for markers of the cell cytoskeleton and the cell polarity confirmed that *Cldn10* KO ameloblasts exhibited an irregular alignment but did not reveal loss of polarity or evident disorganization of the cortical actin compared with WT, with ZO-1–positive TJs at both poles (Fig. 2B; Appendix Fig. 6–7). We investigated the basal TJs at the ultrastructural scale as they are adjacent to the SI cells in which *Cldn10* is deleted. Measurement of their interspace thickness revealed enlarged paracellular spaces between *Cldn10* KO ameloblasts ($P \leq 0.001$) (Fig. 2C). Transmission electron microscopy analysis of the SI showed no differences between KO and WT cells, with desmosomes and gap junctions between the cells (Fig. 2D).

Genes Involved in Ion Transport Are Changed in the Cldn10 KO Enamel Organ

We next investigated the consequences of *Cldn10* deletion on amelogenesis by performing reverse transcription quantitative polymerase chain reaction (RT-qPCR) analysis on laser microdissected ameloblasts and SI cells (Fig. 3A). In ameloblasts, we explored genes related to ion transport and showed that *Slc4a4*, which encodes NBCe1, a sodium bicarbonate cotransporter (Jalali et al. 2014; Bronckers 2017), was significantly decreased in KO ameloblasts. In contrast, the expressions of *Slc20a2* and *Slc27a4*, which encode the inorganic phosphate transporter Pit2 (Merametdjian et al. 2018) and a fatty acid transporter, respectively, were increased in KO ameloblasts compared with WT (Fig. 3A, left panel). We investigated genes related to enamel synthesis by ameloblasts (*Amelx*, *Ambn*, *Mmp20*), which were unchanged, as confirmed at the protein level for amelogenin (Fig. 2B). We also explored the expression of *Cldn1* and *Cldn3*, which encode 2 claudins essential for ameloblast TJ integrity (Bardet et al. 2017). We found a significant decrease in *Cldn3* expression, confirmed at the protein level by immunofluorescence (Appendix Fig. 8).

In the SI, we showed that neither the gene expression related to the noncanonical WNT signaling pathway nor the Notch pathway were changed as a direct consequence of *Cldn10* deletion in SI cells (Fig. 3A, right panel). We investigated the genes related to SI activity, showing that the expression of *Slc4a4* and *Slc20a2*, which encode NBCe1 and Pit2, respectively, were significantly increased in *Cldn10* KO SI cells, while *TrpC6*, which encodes the canonical transient receptor potential 6 that is important for enamel formation (Yang et al. 2017), was decreased. No changes were found for *Alpl*, a marker of the SI (Wang et al. 2020), or for the Sonic Hedgehog pathway. At the protein level, NBCe1 immunolabeling was stronger in the SI and weaker in ameloblasts of KO pups compared with WT (Fig. 3B), whereas alkaline phosphatase (ALP) activity was similar (Appendix Fig. 9).

Enamel Characterization in Epithelium-Targeted Adult Inducible Cldn10 KO Mice

Since (1) the death of *Cldn10* KO pups after a few hours prevents the exploration of the later stages of amelogenesis and enamel and (2) claudin-10 is expressed in the SI throughout all the stages of amelogenesis and in the papillary layer at the maturation stage, we generated inducible *Krt14* $Cre^{+/-}$-*Cldn10* iKO (Cre^{+}) mice. This Cre model is used to target epithelial cells (Vasioukhin et al. 1999), and Keratin 14 is expressed in the dental epithelium (Li et al. 2015) (Appendix Fig. 10). At 2 mo after tamoxifen or vehicle injection induction, we examined the enamel of the lower continuously growing incisor, which formed after *Cldn10* deletion, and of molars, which had formed prior to *Cldn10* deletion. Visual examination showed no striking difference in color or morphology of the incisor between tamoxifen- and vehicle-injected females. However, tamoxifen-injected males exhibited marked white discolored incisors (Fig. 4A). In males, sagittal reconstructions of micro–computed tomography revealed a delayed onset of enamel mineralization, resulting in a significantly lower enamel volume in iKO incisors (Fig. 4B). Consistently, enamel thickness was significantly lower in tamoxifen-induced mice under the distal aspect of the second molar compared with vehicle (Fig. 4D). In addition, enamel density was significantly lower in tamoxifen-induced males compared with vehicle (Fig. 4B). Scanning electron microscopy (SEM) analysis showed well-formed enamel rods in both groups (Fig. 4C and Appendix Fig. 11A). Using energy-dispersive X-ray spectroscopy (EDX), no significant difference was detected in the calcium-to-phosphorus ratio (Appendix Fig. 11B). Nanoindentation showed no difference in Young's modulus or microhardness between animals (Appendix Fig. 11C). Similar investigations were carried out on molars, revealing a significantly lower enamel volume in tamoxifen-induced male mice compared with vehicle with no change in density (Appendix Fig. 12). In contrast, no differences were found between Cre^{+} female mice (Appendix Fig. 13) or similarly treated Cre^{-} animals (Appendix Fig. 14–15). We next evaluated the pH of enamel matrix at the maturation stage. GBHA staining showed 2 red bands in vehicle-treated mice, reflecting the position of smooth-ended maturation ameloblasts (Takano et al. 1982). These bands appeared broader in the *Cldn10 i*KO mice, suggesting a more basic pH (Fig. 4E). Consistently, pH measurement across these bands using BCECF fluorescence (Damkier et al. 2014) showed that the pH was more basic in the *Cldn10* iKO enamel at the proximal part of the maturation zone (proximal band) (Fig. 4E, F). We next investigated the expression of carbonic anhydrase 2 (CA2), the ATP6V1b subunit of the V-ATPase proton pump, and NBCe1, known to be involved in pH regulation during maturation (Lacruz et al. 2017). ATP6V1b and CA2 labeling were increased at the apical border of ameloblasts as well as NBCe1 labeling in the papillary layer in tamoxifen-induced *Cldn10 i*KO animals compared with vehicle (Fig. 4G; Appendix Fig. 16–17).

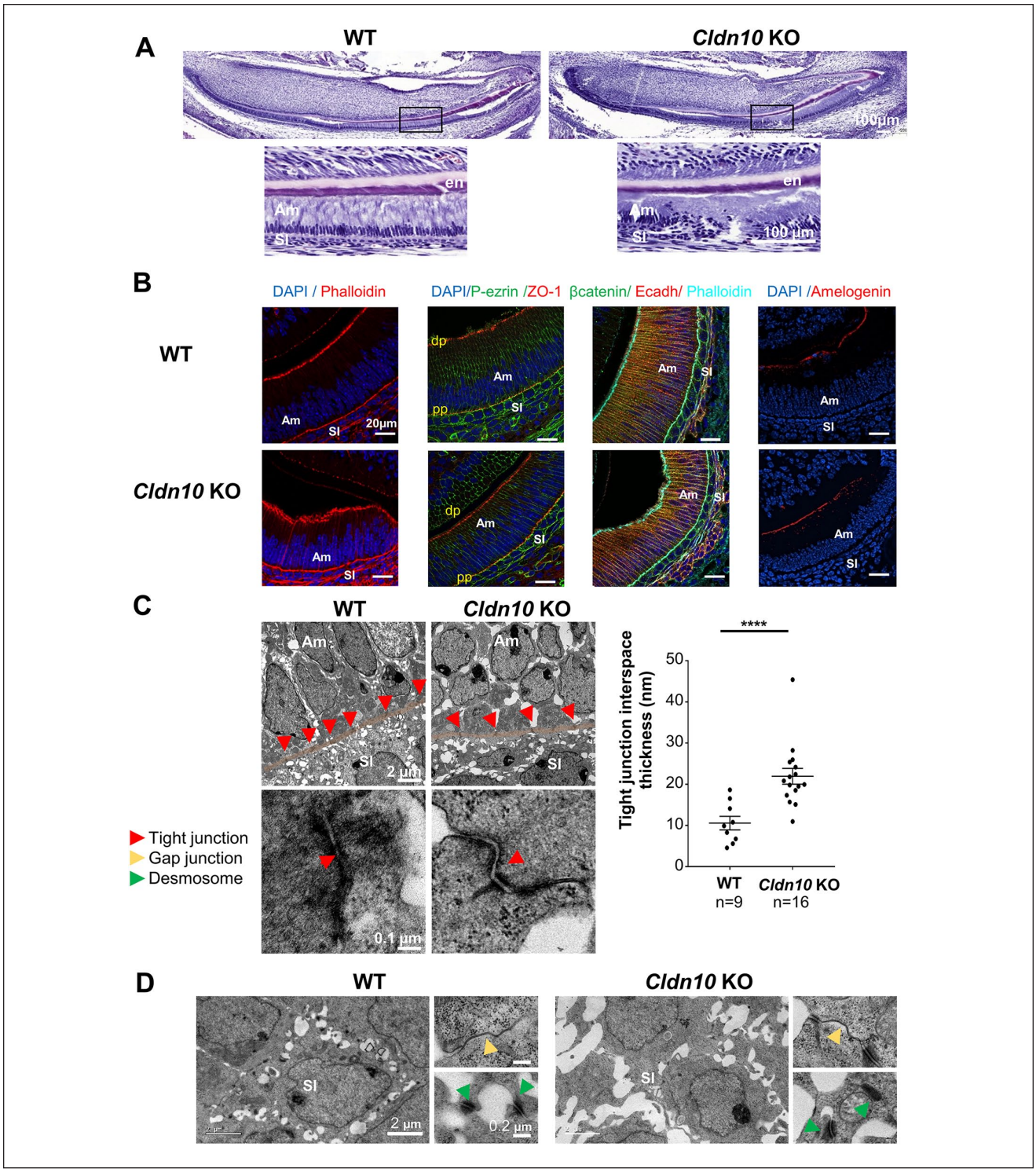

Figure 2. Analysis of the incisor enamel organ in P1 *Cldn10* knockout (KO) mice. (**A**) Hematoxylin and eosin staining of sagittal sections of the P1 incisor showing the organization of secretory stage ameloblasts (Am) associated at their apical end with the forming enamel matrix (e) stained in violet, in *Cldn10* KO and wild-type (WT) pups. Ameloblasts appeared well polarized with a regular nucleus located at the basal end of the cells in WT pups compared with *Cldn10* KO. (**B**) Immunofluorescence analysis of frontal sections of the P1 incisor in *Cldn10* KO and WT mice, claudin-10–ZO-1 co-labeling, phalloidin staining, P-ezrin–ZO-1 co-labeling, β-catenin–E-cadherin and phalloidin co-labeling, and amelogenin staining. (**C**) Tight junction (red arrowhead) imaging by transmission electron microscopy (TEM) at the basal end of secretory ameloblasts from *Cldn10* KO and WT mice. The tight junction (red arrowhead) imaging by TEM was defined by the actin-rich area (orange zone) at the basal end of the secretory ameloblasts. The intercellular spaces at the tight junction level appear to be narrower in WT than in *Cldn10* KO mice. Quantification analysis of tight junction thickness at the basal end of ameloblasts shows a significant increase in tight junction thickness in *Cldn10* KO in comparison with WT mice ($n = 9$ in WT and $n = 15$ in *Cldn10* KO; $P < 0.001$). (**D**) Images of gap junctions and desmosomes in SI. Am, ameloblasts; dp, distal pole of ameloblasts; en, enamel; pp, proximal pole of ameloblasts; SI, stratum intermedium. Red arrowhead: tight junctions; yellow arrowhead: gap junctions; green arrowhead: desmosomes.

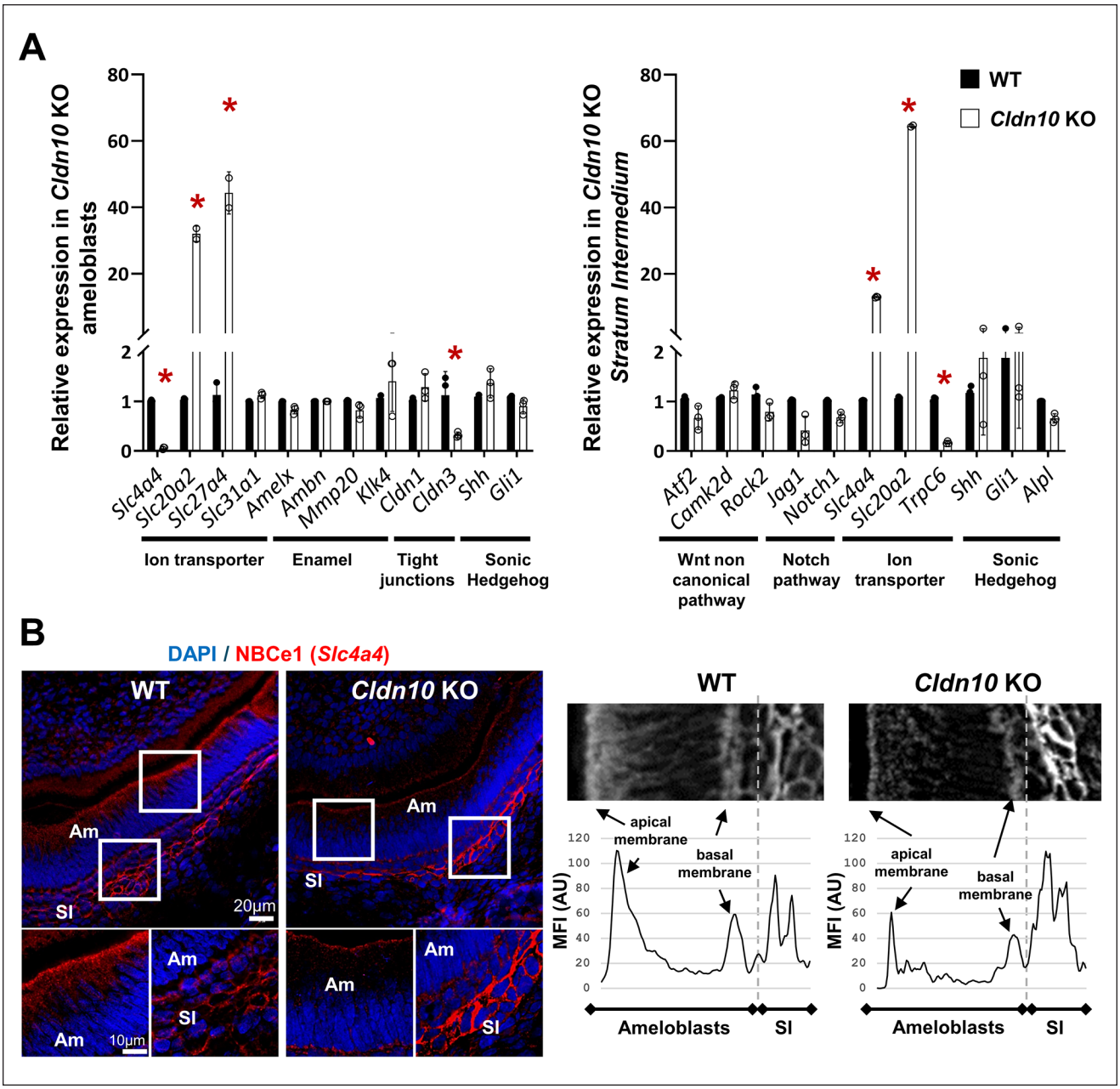

Figure 3. Consequences of *Cldn10* deletion on amelogenesis in P1 *Cldn10* knockout (KO) mice. (**A**) Gene expression of ion transporters (*Slc* family genes and *TrpC6*), *Shh* and *Gli1*, as a stratum intermedium marker, and the Wnt noncanonical pathway with *Atf2*, *Camkd2*, and *Rock2*, and *AmelX*, *Ambn*, *Mmp20*, *KLK4* as ameloblasts markers, and *Cldn1* and *Cldn3* as tight junction markers. (**B**) Immunofluorescence analysis of frontal sections of the P1 incisor in *Cldn10* KO and wild-type (WT) mice with NBCe1 (*Slc4a4*). The right panels represent the mean fluorescence intensity profile plot of a surface projection with a width of 30 µm, perpendicular to the apical membrane of ameloblasts, including ameloblasts and stratum intermedium. In ameloblasts, the NBCe1 labeling is mainly observed at the apical end and is stronger in WT compared with KO ameloblasts. In contrast, the cell membrane of SI is labeled, and the labeling is stronger in KO cells than in WT. Am, ameloblasts; dp, distal pole of ameloblasts; pp, proximal pole of ameloblasts; SI, stratum intermedium.

Enamel Characterization in Transplanted Cldn10 *KO Molar Germs*

We next transplanted molar germs of newborn *Cldn10* KO pups into the kidney capsule of adult WT mice (Fig. 5A). In this model (Jimenez-Rojo and Mitsiadis 2023), the direct effect of the gene deletion on amelogenesis can be studied because the germs develop under normal mineral conditions. Three months upon implantation, a normal tooth with a periodontium formed in both genotypes (Fig. 5B). Enamel examination by SEM (Fig. 5C), EDX (Fig. 5D), and Raman (Fig. 5E) showed no difference between WT and KO germs, except for a slightly

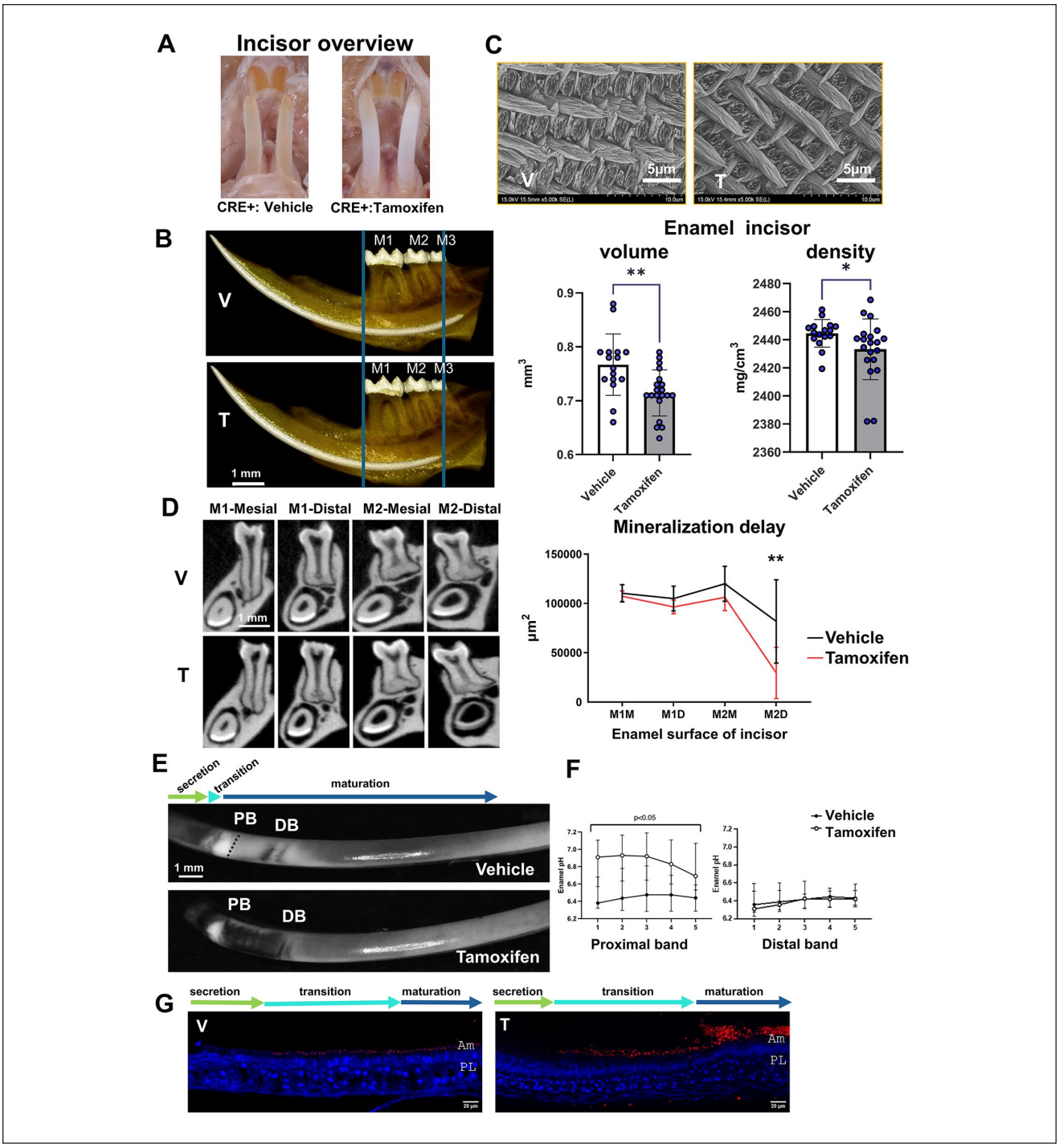

Figure 4. Dental phenotype of adult epithelium-specific inducible male *Cldn10 KO* mice. (**A**) Enamel incisor appearance of tamoxifen-injected compared with vehicle-injected *Krt14- Cre*$^{+/-}$ *Cldn10* iKO mice (Cre^{+} mice). (**B**) Quantitative analyses of high-resolution micro–computed tomography (micro-CT) of mandibular samples showed a significantly lower enamel volume and density in the incisors of activated iKO mice compared with vehicle control ones ($n = 16$ in tamoxifen group vs. $n = 20$ in control group). In control mice, incisor mineralization is observed under the third molar (M3), whereas in activated iKO mice, it is detected under the second molar (M2). (**C**) Scanning electron microscopy analysis of the enamel structure of the incisor at the mesial root of the first molar. (**D**) Quantitative analyses of high-resolution micro-CT of mandibular samples showed a significantly lower incisor enamel surface area under the distal root of M2 of activated *Krt14-Cldn10* iKO mice compared with vehicle-treated mice ($n = 8$ in control group vs. $n = 10$ in activated group), $^{**}P < 0.01$. (**E**) Labial views of lower incisors stained with GBHA showing a proximal band (PB) and a distal band (DB) in the maturation zone of activated iKO mice and vehicle mice. These bands correspond to the region of smooth-ended (SA) maturation ameloblasts. (**F**) Graphs showing the distribution of pH values across the SA bands ($n = 8$ in control group vs. $n = 5$ in activated group). In the proximal band (close to the secretory stage), significantly higher pH values are measured in activated iKO incisors compared with vehicle ones. Data are expressed as median ± interquartile range (IQR). (**G**) ATP6V1B1 immunofluorescence (in red) on sagittal sections of the enamel organ in *Krt14 Cre*$^{+/-}$ *Cldn10* iKO (Cre+) mice with tamoxifen (T) or vehicle (V) injection. Representative pictures showing a stronger labeling at the apical membrane of transition and maturation ameloblasts in tamoxifen-injected animals compared with vehicle ones ($n = 3$ mice per group). Am, ameloblast; de, dentin; en, enamel; M1, first molar; M2, second molar; M3, third molar; PL, apillary layer; T, tamoxifen; V, vehicle.

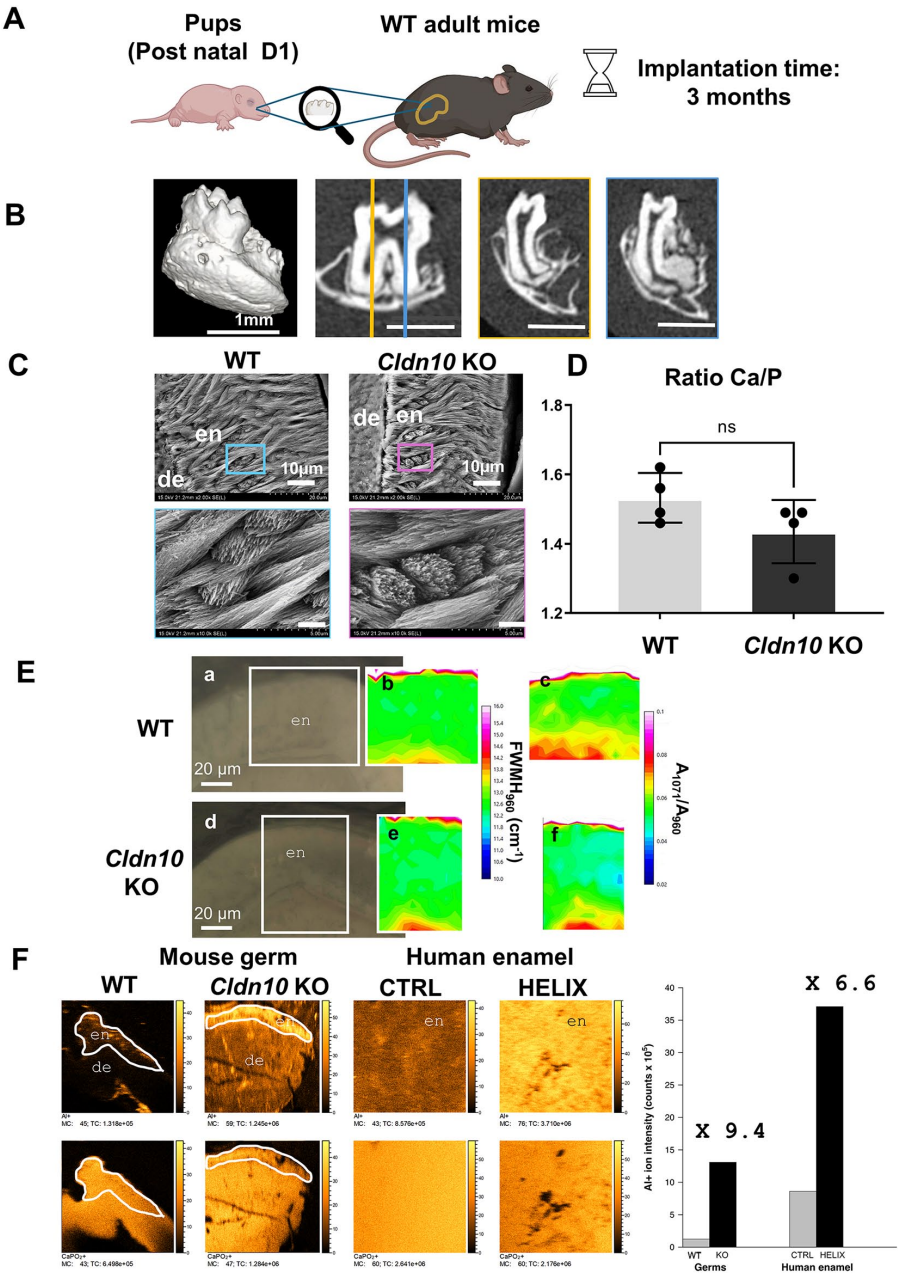

Figure 5. Analysis of the enamel structure of *Cldn10* knockout (KO) molars after transplantation in the kidney capsule. (**A**) Molars germs from *Cldn10* KO and wild-type (WT) mice were harvested at P1 and transplanted in the renal capsule of 3-mo-old WT male mice for 3 mo. (**B**) Two- and 3-dimensional images reconstructed by micro–computed tomography after 3 mo of implantation show a complete molar with full morphology: crown with its 5 cuspids, 2 full-length roots, and surrounding alveolar bone. (**C**) Scanning electron microscopy analyses were performed on the implanted germs, and enamel prisms appeared normal in *Cldn10* KO molars compared with WT ($n = 4$ per group). (**D**) Energy-dispersive X-ray spectroscopy analysis of 3 enamel layers showed a similar calcium/phosphorus (Ca/P) ratio observed in *Cldn10* KO and WT implanted molars ($n = 4$ per group). (**E**) **a, d**: Optical microscopy images of sections of WT and KO samples. The white area delineates the surface mapped by Raman spectroscopy. **b, e**: Raman mapping of the WT and KO samples based on the full width at half maxima (FWHM) of the $\nu(PO_4^{3-})$ vibration band at 960 cm^{-1}, indicative of the crystallinity of the mineral phase. **c, f**: Raman mapping of WT and KO samples based on the ratio between the integrated area of the $\nu(CO_3^{2-})$ and $\nu(PO_4^{3})$ vibration bands at 1,070 cm^{-1} and 960 cm^{-1}, respectively, indicative of the carbonatation rate of hydroxyapatite. Both parameters showed little variations over the whole enamel thickness down to the dentinoenamel junction and did not differ significantly between control and KO samples, indicating that the mineral phase of enamel was of similar crystallinity and carbonatation degree in the 2 types of teeth. (**F**) Time-of-flight secondary ion mass spectrometry ion images of Al^+ m/z 26.98 and of $CaPO_2^+$ m/z 102.92 cations detected at the surface of the sample surfaces. Field of view 500 µm × 500 µm, 256 × 256 pixels, pixel size 1.95 µm. All images recorded with the same primary ion fluence of 5.1 × 1,011 ions cm^{-2}. Color scale bars, with amplitude in number of counts, are indicated to the right of each ion image. The amplitude of the color scale corresponds to the maximum number of counts (MC) and could be read as [0, MC]. TC is the total number of counts recorded for the specified m/z (sum of counts in all the pixels). The TC values for Al^{3+} are gathered on the graph, highlighting the higher abundancy of this element in (1) enamel (defined by a white line) from germs of KO mice compared with WT, (2) enamel from the HELIX patient compared with control. de, dentin; en, enamel.

lower value of Cl content in the KO germs (Appendix Fig. 18). However, time-of-flight secondary ion mass spectrometry (TOF-SIMS), a highly sensitive method for chemical analysis and imaging of biological tissues (Van Nuffel and Brunelle 2022), revealed a higher level of aluminum species in KO germs compared with WT (×9.4). Ultimately, we assessed this finding in a HELIX tooth collected before tooth eruption (Obtel et al. 2022) and found a larger amount of this element in the enamel compared with a gender- and age-matched control tooth (×6.6) (Fig. 5F). Other elements, such as calcium, strontium, and magnesium, were increased in the murine KO germs compared with WT, but no difference was observed in the human enamel (Appendix Table 1).

Discussion

Accumulating data have shown that *Cldn10*/claudin-10 is expressed in the enamel organ since the early stages of amelogenesis, specifically in the SI, where it has been proposed to be a marker of dental epithelial cells (Ohazama and Sharpe 2007; Chiba et al. 2020; Wang et al. 2020). Our data demonstrate that claudin-10 is indeed located in the SI, in the cell membrane but not at the TJs. In the kidney, claudin-10 has been shown to be present in the TJs of a subset of medullary and cortical TAL cells, where it acts as a selective cation channel but also in other non–TJ-associated membrane domains (Prot-Bertoye et al. 2021; Meoli and Gunzel 2023). This latter observation is consistent with our findings in the SI; however, in both systems, the exact role of non–TJ-associated claudin-10 remains to be elucidated. Furthermore, our data show that claudin-10 is expressed in the papillary layer at the maturation stage.

At the secretion stage, the expression of several molecules involved in the ion transport and pH regulation of the enamel matrix was altered in both the *Cldn10* KO SI cells and ameloblasts. Since claudin-10 is expressed in SI but not in ameloblasts, our data show that *Cldn10* deletion has direct effects on the SI and indirect effects on ameloblasts. In addition, at the maturation stage, proteins involved in pH regulation were changed in ameloblasts and in the papillary layer, also indicating direct and indirect effects of *Cldn10* deletion.

We found that the expression of *Slc4a4*, which encodes NBCe1, a bicarbonate sodium cotransporter, was significantly increased in the SI, whereas it was decreased in the ameloblasts, in KO mice, compared with WT. It was also increased in the papillary layer at the maturation stage in adult conditional mice. NBCe1 is important for enamel matrix pH regulation (Jalali et al. 2014), and pathogenic variants of *SLC4A4* have been linked to AI in patients with proximal renal tubular acidosis (Kantaputra et al. 2022). Follow-up of incisor growth in adult male mice with tamoxifen-induced *Cldn10* silencing showed that enamel volume was reduced, concomitantly with an increase of pH in the enamel matrix at the early stages of maturation. This finding is in sharp contrast with our report on claudin-16, a cation-selective intercellular pore located in the apical TJs of secretory ameloblasts, the expression of which is required for high paracellular permeability to Ca^{2+} and Mg^{2+} and for which deletion is associated with an acidic pH of enamel matrix (Bardet et al. 2016). These data suggest that both claudin-16 and claudin-10 may contribute to pH regulation during amelogenesis with opposite roles. Noteworthy, it has been shown that, in the TAL, claudin-10 expression at TJs almost never overlapped with that of claudin-16 and claudin-19 (Brideau et al. 2024).

The exploration of amelogenesis in constitutive *Cldn10* KO mice was partially hampered by the premature death of the pups a couple of hours after birth (Breiderhoff et al. 2012). In these pups, the enamel organ appeared disorganized but the enamel matrix was still forming, and secretory ameloblasts maintained their organization (cytoskeleton, polarity, junctions). Consistent with this observation, the exploration of enamel in the molar germ transplantation model and in the tamoxifen-induced *Cldn10* KO adult male mice did not reveal significant disturbances, as evidenced by a well-distinguishable decussating prism pattern and normal Ca/P ratio. However, in tamoxifen-induced KO male mice, the enamel of the continuously growing incisors was discolored, suggesting a loss of iron uptake, which may result in an enamel less resistant to posteruptive acidic challenges (Srot et al. 2024). It is noteworthy that HELIX syndrome affects both genders in a similar manner (Hadj-Rabia et al. 2018), and the differences observed here between male and female Cre mice may be due to the construction of this CreERT model (Vasioukhin et al. 1999).

It has been previously reported that *Adam10* deletion in the dental epithelium induced downregulation of Notch1 expression, leading to loss of the SI layer and ALP activity and disorganization of ameloblasts (Mitsiadis et al. 2022). Here, our RT-qPCR analysis showed no change in the Notch pathway in the *Cldn10* KO SI. In addition, ALP activity remained robust in *Cldn10* KO SI. Therefore, in contrast to *Adam10* (Mitsiadis et al. 2022), *Cldn10* deletion does not significantly alter the Notch pathway, resulting in the maintenance of the SI layer. However, it seems relevant in the future to generate conditional models that target more specifically the various development stages of the dental epithelium (Yu and Klein 2020), for example, by generating a *Notch1*-CRE mouse for the SI (Mitsiadis et al. 2022).

We found a lower enamel volume in the molars of the activated *Krt14-Cldn10* iKO male mice compared with the vehicle. Since *Cldn10* deletion occurred long after molar eruption, this indicates exacerbated enamel wear due to salivary deficiency. The discoloration of the erupted enamel of the lower incisors in these mice may also result from hyposalivation. Our data are consistent with the decreased claudin-10 expression in NOD mice, a model of Sjögren's syndrome, associated with hyposalivation (Scuron et al. 2019; He et al. 2024). Progressive enamel erosion has been shown in the molars of NOD mice (Tulek et al. 2020), which is consistent with our findings in the erupted enamel of the conditional KO mice and in HELIX patients (Hadj-Rabia et al. 2018).

Our recent investigation of a HELIX third molar, which had not yet erupted, revealed no significant abnormality in the enamel structure (Obtel et al. 2022), consistent with our present findings in the preeruptive incisor of the Cre-Lox model and in the transplanted germs. These data suggest that salivary

dysfunction is the primary cause of the rapid enamel wear associated with HELIX.

TOF-SIMS imaging (Bich et al. 2013) revealed high aluminum content in the enamel of the HELIX tooth and *Cldn10* KO germs that had mineralized upon implantation in WT mice. Although widely distributed in body fluids including blood, aluminum is considered an adventitious element present in food and water, with no known biological function (Exley and Mold 2015). In France, tap water contains about 16 µg/mL of aluminum (Le Bot et al. 2016), meaning that both mice and patients reported here were chronically exposed to aluminum during amelogenesis. Our data show that diffusion of aluminum through the enamel organ was greater in the *Cldn10*-deficient implanted germs and patient, suggesting a loss of enamel organ integrity in the absence of claudin-10.

Aluminum ions originating from the blood vessels adjacent to the outer layer of the enamel organ must go across its cell layers to reach the enamel matrix. Little is known about aluminum ion transport, which appears to occur by both transcellular and paracellular routes (Exley and Mold 2015). Enlargement of the basal TJs in *Cldn10* KO ameloblasts together with the decreased expression of claudin-3, a sealing claudin, may be consistent with an increased paracellular transport of aluminum. Furthermore, the presence of aluminum in enamel, either integrated to the hydroxyapatite crystals or not (Chappard et al. 2016), may not increase its solubility (Kleber and Putt 1985) and is therefore unlikely to contribute to its fragility. It will be important to measure the levels of aluminum in other HELIX/*Cldn10* KO tissues as, for example, the brain, where it has been shown to be neurotoxic (Kumar and Gill 2009).

In *Cldn10* KO pups, we showed that the expression of NBCe1 was increased in the SI and decreased in the ameloblasts, suggesting a role of claudin-10 in acid and base transport. This finding is consistent with the basic pH measured in the proximal part (adjacent to secretion) of the tamoxifen-induced *Cldn10* KO incisors at the maturation stage. However, we do not have an explanation for the overexpression of ATP6V1B1 at the apical membrane of iKO ameloblasts at the maturation stage. The exact mechanisms underlying this pH regulation need to be further investigated by functional studies in other organs that are easier to investigate than the enamel organ, such as the renal tissue, or by using acid and base transport inhibitors.

Conclusions

Our data demonstrate that claudin-10 is expressed in the cellular membrane of the SI where it contributes to the integrity of the enamel organ, directly in the SI and indirectly in ameloblasts. In its absence, enamel forms properly despite a basic pH of enamel matrix at early maturation stage, suggesting a role of claudin-10 in acid-base regulation of the enamel organ. Overall, xerostomia appears to be the main culprit for enamel wear observed in HELIX patients.

Author Contributions

T.N. Nguyen, C. Andrique, M. Requin, contributed to design, data acquisition, analysis, and interpretation, drafted and critically revised the manuscript; S. Ribes, N. Brouilly, A. Kiesow, A. Brunelle, A. Percot, S. Hadj-Rabia, C. Gaucher, F. Ramirez Rozzi, T. Coradin, contributed to design, data acquisition, analysis, and interpretation, critically revised the manuscript; J. Bouchet, contributed to design, data analysis and interpretation, drafted and critically revised the manuscript; N. Obtel, C. Torrens, A. Schmitt, T. Guilbert, contributed to design, data acquisition and analysis, critically revised the manuscript; L. Slimani, contributed to design, data acquisition, critically revised the manuscript; M. Morawietz, C. Bardet, D. Muller, contributed to design, data interpretation, critically revised the manuscript; A. Le Bivic, P. Houillier, contributed to conception, design, data acquisition, analysis, and interpretation, critically revised the manuscript; T. Breiderhoff, C. Chaussain, contributed to conception, design, data analysis and interpretation, drafted and critically revised the manuscript. All authors gave final approval and agree to be accountable for all aspects of the work.

Acknowledgments

The authors thank Dr. Olivier Duverger (National Institutes of Health, Bethesda, MD, USA) for helpful discussion regarding the tooth germ transplantation model. We thank David Montero from the Institut des Matériaux de Paris Centre (IMPC FR2482) for servicing field emission gun SEM and EDX instrumentation and Sorbonne Université, CNRS, and C'Nano projects of the Région Ile-de-France for funding (Paris, France).

Declaration of Conflicting Interests

The authors declared no potential conflicts of interest with respect to the research, authorship, and/or publication of this article.

Funding

The authors disclosed receipt of the following financial support for the research, authorship, and/or publication of this article: This study received financial support from Université Paris Cité and from the T-JUST program (ANR-17CE14-0032-02). The Nghia Nguyen PhD was supported by the Ambassade de France in Vietnam. The IBDM imaging facility, member of the national infrastructure France-BioImaging is supported by the French National Research Agency (ANR-10-INBS-04 & ANR-10-INSB-04-01call "investissements d'Avenir"). MR and ALB salaries are supported by CNRS (Centre National de la Recherche Scientifique). IMAG'IC core facility (Institut Cochin) is part of the National Infrastructure France-BioImaging supported by the French National Research Agency (ANR-10-INBS-04). The electron microscopy experiments were performed on the PiCSL-FBI core facility (IBDM, AMU-Marseille), member of the France-BioImaging national research infrastructure (ANR-10-INBS-04) and member of the Marseille Imaging Institute, an Excellence Initiative of Aix Marseille University A*MIDEX, a French "Investissements d'Avenir" programme (AMX 19 IET 002).

ORCID iDs

T.N. Nguyen https://orcid.org/0000-0003-2848-242X
C. Andrique https://orcid.org/0000-0002-0447-9616
J. Bouchet https://orcid.org/0000-0002-6611-4380
T. Guilbert https://orcid.org/0000-0001-5069-0730
A. Brunelle https://orcid.org/0000-0001-6526-6481
A. Percot https://orcid.org/0000-0002-3896-314X
T. Coradin https://orcid.org/0000-0003-3374-5722
T. Breiderhoff https://orcid.org/0000-0002-1676-7498

Data Availability

The data that support the findings of this study are available on request from the corresponding author.

References

Bardet C, Courson F, Wu Y, Khaddam M, Salmon B, Ribes S, Thumfart J, Yamaguti PM, Rochefort GY, Figueres ML, et al. 2016. Claudin-16 deficiency impairs tight junction function in ameloblasts, leading to abnormal enamel formation. J Bone Miner Res. 31(3):498–513.

Bardet C, Ribes S, Wu Y, Diallo MT, Salmon B, Breiderhoff T, Houillier P, Müller D, Chaussain C. 2017. Claudin loss-of-function disrupts tight junctions and impairs amelogenesis. Front Physiol. 8:326. doi:10.3389/fphys.2017.00326

Bich C, Touboul D, Brunelle A (2013). Study of experimental variability in TOF-SIMS mass spectrometry imaging of biological samples.

Breiderhoff T, Himmerkus N, Stuiver M, Mutig K, Will C, Meij IC, Bachmann S, Bleich M, Willnow TE, Müller D. 2012. Deletion of claudin-10 (Cldn10) in the thick ascending limb impairs paracellular sodium permeability and leads to hypermagnesemia and nephrocalcinosis. Proc Natl Acad Sci U S A. 109(35):14241–14246.

Brideau G, Cheval L, Griveau C, Ling WE, Lievre L, Crambert G, Müller D, Broćić J, Cherchame E, Houillier P, et al. 2024. Claudin-10 expression and the gene expression pattern of thick ascending limb cells. Int J Mol Sci. 25(7):4008.

Bronckers AL. 2017. Ion transport by ameloblasts during amelogenesis. J Dent Res. 96(3):243–253.

Chappard D, Bizot P, Mabilleau G, Hubert L. 2016. Aluminum and bone: review of new clinical circumstances associated with Al(3+) deposition in the calcified matrix of bone. Morphologie. 100(329):95–105.

Chiba Y, Saito K, Martin D, Boger ET, Rhodes C, Yoshizaki K, Nakamura T, Yamada A, Morell RJ, Yamada Y, et al. 2020. Single-cell RNA-sequencing from mouse incisor reveals dental epithelial cell-type specific genes. Front Cell Dev Biol. 8:841. doi:10.3389/fcell.2020.00841

Damkier HH, Josephsen K, Takano Y, Zahn D, Fejerskov O, Frische S. 2014. Fluctuations in surface pH of maturing rat incisor enamel are a result of cycles of H(+)-secretion by ameloblasts and variations in enamel buffer characteristics. Bone. 60:227–234.

Exley C, Mold MJ. 2015. The binding, transport and fate of aluminium in biological cells. J Trace Elem Med Biol. 30:90–95.

Gunzel D, Stuiver M, Kausalya PJ, Haisch L, Krug SM, Rosenthal R, Meij IC, Hunziker W, Fromm M, Müller D. 2009. Claudin-10 exists in six alternatively spliced isoforms that exhibit distinct localization and function. J Cell Sci. 122(Pt 10):1507–1517.

Hadj-Rabia S, Brideau G, Al-Sarraj Y, Maroun RC, Figueres ML, Leclerc-Mercier S, Olinger E, Baron S, Chaussain C, Nochy D, et al. 2018. Multiplex epithelium dysfunction due to CLDN10 mutation: the HELIX syndrome. Genet Med. 20(2):190–201.

He L, Yuan SZ, Mao XD, Zhao YW, He QH, Zhang Y, Su JZ, Wu LL, Yu GY, Cong X. 2024. Claudin-10 decrease in the submandibular gland contributes to xerostomia. J Dent Res. 103(2):167–176.

Jalali R, Guo J, Zandieh-Doulabi B, Bervoets TJ, Paine ML, Boron WF, Parker MD, Bijvelds MJ, Medina JF, DenBesten PK, et al. 2014. NBCe1 (SLC4A4) a potential pH regulator in enamel organ cells during enamel development in the mouse. Cell Tissue Res. 358(2):433–442.

Jimenez-Rojo L, Mitsiadis TA. 2023. Kidney capsule transplantation of chemically treated embryonic murine tooth germs. STAR Protoc. 4(3):102377. doi:10.1016/j.xpro.2023.102377

Kantaputra P, Guven Y, Aksu B, Kalayci T, Dogan C, Intachai W, Olsen B, Tongsima S, Ngamphiw C, Noppakun K. 2022. Distal renal tubular acidosis, autoimmune thyroiditis, enamel hypomaturation, and tooth agenesis caused by homozygosity of a novel double-nucleotide substitution in SLC4A4. J Am Dent Assoc. 153(7):668–676.

Klar J, Piontek J, Milatz S, Tariq M, Jameel M, Breiderhoff T, Schuster J, Fatima A, Asif M, Sher M, et al. 2017. Altered paracellular cation permeability due to a rare CLDN10B variant causes anhidrosis and kidney damage. PLoS Genet. 13(7):e1006897. doi:10.1371/journal.pgen.1006897

Kleber CJ, Putt MS. 1985. Uptake and retention of aluminum by dental enamel. J Dent Res. 64(12):1374–1376.

Kumar V, Gill KD. 2009. Aluminium neurotoxicity: neurobehavioural and oxidative aspects. Arch Toxicol. 83(11):965–978.

Lacruz RS, Habelitz S, Wright JT, Paine ML. 2017. Dental enamel formation and implications for oral health and disease. Physiol Rev. 97(3):939–993.

Le Bot B, Lucas JP, Lacroix F, Glorennec P. 2016. Exposure of children to metals via tap water ingestion at home: contamination and exposure data from a nationwide survey in France. Environ Int. 94:500–507.

Li S, Ge S, Yang P. 2015. Expression of cytokeratins in enamel organ, junctional epithelium and epithelial cell rests of Malassez. J Periodontal Res. 50(6):846–854.

Liu H, Yan X, Pandya M, Luan X, Diekwisch TG. 2016. Daughters of the enamel organ: development, fate, and function of the stratum intermedium, stellate reticulum, and outer enamel epithelium. Stem Cells Dev. 25(20):1580–1590.

Meoli L, Gunzel D. 2023. The role of claudins in homeostasis. Nat Rev Nephrol. 19(9):587–603.

Merametdjian L, Beck-Cormier S, Bon N, Couasnay G, Sourice S, Guicheux J, Gaucher C, Beck L. 2018. Expression of phosphate transporters during dental mineralization. J Dent Res. 97(2):209–217.

Milatz S. 2019. A novel claudinopathy based on claudin-10 mutations. Int J Mol Sci. 20(21):5396. doi:10.3390/ijms20215396

Mitsiadis TA, Jimenez-Rojo L, Balic A, Weber S, Saftig P, Pagella P. 2022. Adam10-dependent Notch signaling establishes dental epithelial cell boundaries required for enamel formation. iScience. 25(10):105154. doi:10.1016/j.isci.2022.105154

Obtel N, Le Cabec A, Nguyen TN, Giabicani E, Van Malderen SJM, Garrevoet J, Percot A, Paris C, Dean C, Hadj-Rabia S, et al. 2022. Impact of claudin-10 deficiency on amelogenesis: lesson from a HELIX tooth. Ann N York Acad Sci. 1516(1):197–211.

Ohazama A, Sharpe PT. 2007. Expression of claudins in murine tooth development. Dev Dyn. 236(1):290–294.

Prot-Bertoye C, Griveau C, Skjodt K, Cheval L, Brideau G, Lievre L, Ferriere E, Arbaretaz F, Garbin K, Zamani R, et al. 2021. Differential localization patterns of claudin 10, 16, and 19 in human, mouse, and rat renal tubular epithelia. Am J Physiol Renal Physiol. 321(2):F207–F224.

Scuron MD, Fay B, Oliver J, Smith P. 2019. Spontaneous model of Sjogren's syndrome in NOD mice. Curr Protoc Pharmacol. 86(1):e65. doi:10.1002/cpph.65

Srot V, Houari S, Kapun G, Bussmann B, Predel F, Pokorny B, Bužan E, Salzberger U, Fenk B, Kelsch M, et al. 2024. Ingenious architecture and coloration generation in enamel of rodent teeth. ACS Nano. 18(17):11270–11283.

Takano Y, Crenshaw MA, Bawden JW, Hammarstrom L, Lindskog S. 1982. The visualization of the patterns of ameloblast modulation by the glyoxal bis(2-hydroxyanil) staining method. J Dent Res. 1580–1587.

Tulek A, Mulic A, Refsholt Stenhagen K, Galtung HK, Saeed M, Utheim TP, Khuu C, Galteland P, Sehic A. 2020. Dental erosion in mice with impaired salivary gland function. Acta Odontol Scand. 78(5):390–400.

Van Nuffel S, Brunelle A. 2022. TOF-SIMS imaging of biological tissue sections and structural determination using tandem MS. Methods Mol Biol. 2437:77–86.

Vasioukhin V, Degenstein L, Wise B, Fuchs E. 1999. The magical touch: genome targeting in epidermal stem cells induced by tamoxifen application to mouse skin. Proc Natl Acad Sci U S A. 96(15):8551–8556.

Wang X, Chiba Y, Jia L, Yoshizaki K, Saito K, Yamada A, Qin M, Fukumoto S. 2020. Expression patterns of claudin family members during tooth development and the role of claudin-10 (Cldn10) in cytodifferentiation of stratum intermedium. Front Cell Dev Biol. 8:595593. doi:10.3389/fcell.2020.595593

Yamaguti PM, Neves FA, Hotton D, Bardet C, de La Dure-Molla M, Castro LC, Scher MD, Barbosa ME, Ditsch C, Fricain JC, et al. 2017. Amelogenesis imperfecta in familial hypomagnesaemia and hypercalciuria with nephrocalcinosis caused by CLDN19 gene mutations. J Med Genet. 54(1):26–37.

Yang J, Cai W, Lu X, Liu S, Zhao S. 2017. RNA-sequencing analyses demonstrate the involvement of canonical transient receptor potential channels in rat tooth germ development. Front Physiol. 8:455. doi:10.3389/fphys.2017.00455

Yu T, Klein OD. 2020. Molecular and cellular mechanisms of tooth development, homeostasis and repair. Development. 147(2):dev184754. doi:10.1242/dev.184754